

VLM-AD: End-to-End Autonomous Driving through Vision-Language Model Supervision

Yi Xu^{*1,2} Yuxin Hu¹ Zaiwei Zhang¹ Gregory P. Meyer¹
 Siva Karthik Mustikovela¹ Siddhartha Srinivasa¹ Eric M. Wolff¹ Xin Huang¹
¹Cruise LLC ²Northeastern University
 xu.yi@northeastern.edu, cyrus.huang@getcruise.com

Abstract

Human drivers rely on commonsense reasoning to navigate diverse and dynamic real-world scenarios. Existing end-to-end (E2E) autonomous driving (AD) models are typically optimized to mimic driving patterns observed in data, without capturing the underlying reasoning processes. This limitation constrains their ability to handle challenging driving scenarios. To close this gap, we propose VLM-AD, a method that leverages vision-language models (VLMs) as teachers to enhance training by providing additional supervision that incorporates unstructured reasoning information and structured action labels. Such supervision enhances the model’s ability to learn richer feature representations that capture the rationale behind driving patterns. Importantly, our method does not require a VLM during inference, making it practical for real-time deployment. When integrated with state-of-the-art methods, VLM-AD achieves significant improvements in planning accuracy and reduced collision rates on the nuScenes dataset.

1. Introduction

End-to-end autonomous driving (AD) unifies perception, prediction, and planning into a single framework. This integration aims to coordinate multiple complex tasks, including detection, tracking, mapping, prediction, and planning. Recent approaches [17, 18, 26] have tackled these challenges by using sensor data to generate planned ego trajectories with a single, holistic model. Although these methods have shown promising results, their performance degrades in challenging, long-tail events [5, 7]. On the other hand, human drivers often handle such scenarios effectively, by reasoning through the driving environment and adapting their actions accordingly. This highlights a training gap in current E2E models, which rely solely on the trajectory supervision as sequences of points, lacking the reasoning

^{*}Work done during Yi’s internship at Cruise LLC.

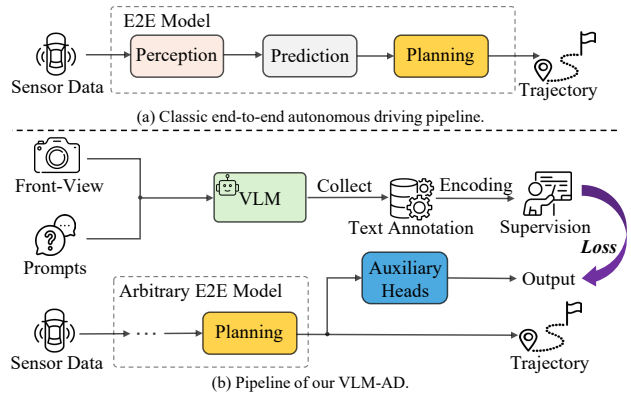


Figure 1. VLM-AD augments an arbitrary end-to-end driving model using auxiliary text prediction tasks during training. These tasks distill driving reasoning knowledge from a VLM to encourage the model to learn richer representations, without fine-tuning a VLM at training time or requiring a VLM at inference time.

information necessary for learning rich and robust feature representations to achieve better driving performance.

Manual annotation of reasoning information is often costly, time-consuming, and prone to inconsistent and subjective results, making it difficult to obtain high-quality and scalable annotations. Large foundation models offer an alternative by providing their reasoning capabilities for complex tasks such as driving. Recent methods [4, 13, 20, 27, 39, 40, 51, 54, 55, 61] have directly integrated large foundation models, such as large language models (LLMs) [12, 44, 52] and vision-language models (VLMs) [31, 32, 36, 45], into AD systems to leverage their reasoning capabilities. However, these methods require extensive fine-tuning to translate language-based outputs into precise numerical results, such as planned trajectories or control signals. In addition, these methods rely on large foundation models during inference, which significantly increases both training costs and inference time, making these methods impractical for real-world applications

Given the limitations of manual annotation and the challenges of directly integrating large foundation models into driving systems, we pose the following question: Can large foundation models, such as VLMs, generate reasoning-based text information to enhance autonomous driving models without requiring integration at inference time?

Motivated by this question, we propose VLM-AD, illustrated in Fig. 1, a novel method that leverages VLMs as teachers to automatically generate reasoning-based text annotations. These annotations then serve as supplementary supervisory signals to train end-to-end pipelines, extending beyond standard trajectory labels. Specifically, given a sequence of multi-view images and the future trajectory of the ego vehicle, we project the future trajectory onto the initial front-view image to incorporate critical temporal movement information. We then prompt the VLM model with targeted questions regarding the vehicle’s current status, intended future actions, and reasoning process to generate both freeform and structured responses, thus infusing critical VLM knowledge into the training pipeline.

This scalable approach enables us to build a dataset enriched with VLM-generated annotations, effectively addressing the absence of reasoning cues in existing driving datasets. We design auxiliary tasks based on these annotations and integrate them seamlessly into existing end-to-end models for joint training. These tasks encourage the model to learn richer feature representations for improved driving performance, without requiring VLM involvement at inference time. Our contributions can be summarized as follows:

- We propose VLM-AD, a simple yet effective approach that distills driving reasoning knowledge from VLMs into end-to-end AD pipelines through a high-quality dataset of reasoning-based behavioral text annotations, generated through carefully crafted prompts directed to VLMs.
- We design two plug-and-play auxiliary tasks to supervise existing end-to-end AD pipelines through both unstructured freeform text and structured action labels. These tasks enable effective distillation of VLM knowledge, guiding the model to learn richer feature representations for improved planning performance, without requiring VLM fine-tuning or inference-time usage.
- Extensive experiments on the nuScenes dataset validate the effectiveness of our proposed method, showing significant improvements of 14.6% and 33.3% in L2 planning error, and reductions in collision rate by 38.7% and 57.4% for UniAD and VAD, respectively.

2. Related Work

End-to-End Autonomous Driving. End-to-end autonomous driving systems jointly train all modules toward a unified goal, resulting in reduced information loss throughout the pipeline. Unified frameworks such as ST-P3 [17] and UniAD [18] propose vision-based end-to-end AD sys-

tems that unify perception, prediction, and planning. These models achieve state-of-the-art results on the open-loop nuScenes dataset [3]. Following works, such as VAD [26] and VADv2 [6], introduce a vectorized encoding approach for efficient scene representation and extend to closed-loop simulation on CARLA [14]. Recent methods like Ego-MLP [62], BEV-Planner [35], and PARA-Drive [58] have been developed to explore ego-status and novel design spaces within modular stacks to further enhance driving performance. While E2E driving models show promising results in the development of E2E driving methods, they are primarily optimized to mimic driving patterns in the data, without capturing the underlying reasoning processes. This limitation is largely due to the lack of reasoning information in existing datasets. Consequently, these methods are unable to acquire deeper reasoning knowledge, which could limit their performance in challenging scenarios.

Foundation Models for Autonomous Driving. Foundation models, including large-language models (LLMs) and vision-language models (VLMs), are being increasingly applied in autonomous driving to leverage their advanced reasoning capabilities. GPT-Driver [39] and Driving-with-LLMs [4] use LLMs to provide action recommendations with explanations, thus enhancing decision transparency. A recent approach [11] leverages LLMs to evaluate lane occupancy and safety, enabling more human-like intuitive scene understanding. However, LLM-based methods primarily rely on language inputs, which limits their potential to incorporate rich visual features essential for driving.

VLMs address this gap by integrating language and vision for multimodal reasoning, supporting tasks like scene understanding [10, 21, 42, 49] and data generation [24, 56, 64]. VLMs have also been used for unified navigation and planning [15, 29, 51, 53] as well as end-to-end autonomous driving [27, 40, 55, 61]. However, existing VLM-based methods often require extensive domain-specific fine-tuning, which significantly increases computational cost and inference latency. Closely related to our method in end-to-end autonomous driving, VLP [40] transforms ground-truth trajectory and bounding box labels into text features for contrastive learning, but it does not introduce information beyond existing supervision labels. In contrast, our method leverages VLMs to provide additional reasoning information to further enhance driving performance.

Multi-Task Learning. Multi-task learning (MTL) jointly performs several related tasks using a shared representation through separate branches or heads. This approach leverages shared domain knowledge, enhancing feature robustness and generalization, making it well-suited for end-to-end autonomous driving. In AD systems, auxiliary tasks such as semantic segmentation [9, 19, 23, 33, 60], depth estimation [33, 60], HD mapping and BEV segmentation [8, 25, 47, 48, 63] are commonly adopted to extract

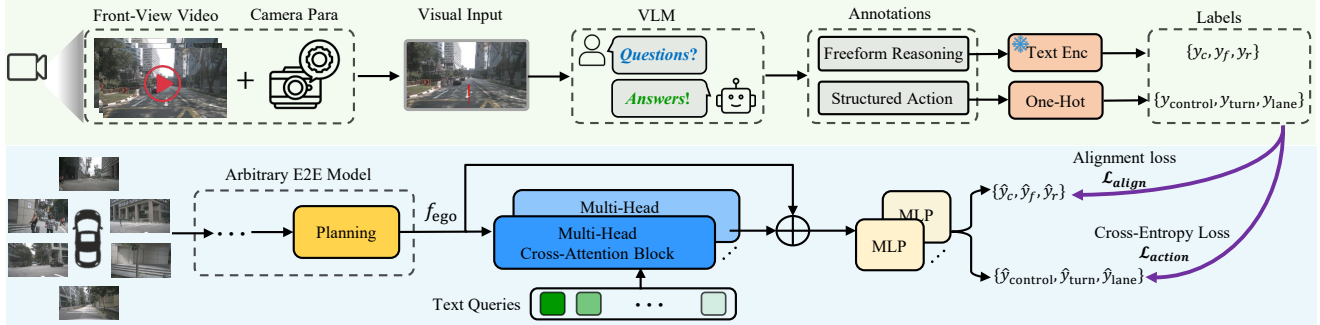


Figure 2. Framework of our proposed VLM-AD. We leverage a VLM as a teacher to generate both freeform reasoning and structured action annotations, which are converted into supervisory signals to enable the model to learn richer representations through auxiliary text alignment and action classification heads. As a result, our method offers better planning results and interpretable action predictions, without requiring a VLM at inference time.

meaningful perception representations for subsequent objects. Beyond vision tasks, other methods [22, 59] predict additional traffic light states or control signals, to improve driving performance. Inspired by the success of multi-task learning, we design novel auxiliary tasks to encourage the model to learn richer feature representations through high-quality reasoning annotations from VLMs, ultimately leading to more reliable planning performance.

3. Method

Fig. 2 presents an overview of our proposed VLM-AD framework, which consists of two main components. The first is the annotation branch, where we leverage the VLM to generate additional information, creating a supplementary dataset that serves as supervision. The second component is our designed auxiliary heads, which aim to align with this additional supervision and can be effectively integrated into any E2E model following the planning module.

3.1. VLM Text Annotation

Fig. 3 illustrates the annotation process, where we utilize a VLM as the teacher to enrich the dataset with additional information, leveraging its reasoning capabilities from visual inputs to deepen an E2E model’s understanding of driving behaviors. The annotation process can be defined as:

$$\mathcal{A} = \mathcal{M}(\mathcal{P}, \mathcal{V}), \quad (1)$$

where $\mathcal{M}(\cdot)$ represents the VLM model, \mathcal{P} denotes the language prompts, \mathcal{V} is the visual input, and \mathcal{A} is the model’s natural language output, serving as annotations for the dataset. Our goal is to provide images captured from the ego vehicle’s camera, along with specifically crafted prompts, to obtain detailed informative responses from the VLM, leveraging its extensive world knowledge.

In our work, we employ GPT-4o [2], a high-performance VLM trained on internet-scale data, to automatically anno-

tate our dataset. GPT-4o can interpret the scenario, generate suitable reasoning-based responses, and accurately identify the actions of the ego vehicle in complex scenarios.

Visual Input. When determining the visual input, we encounter two challenges. The first challenge is selecting the appropriate image(s) from multiple cameras that provide 360-degree coverage around the ego vehicle. We explore two approaches: creating a composite large image from all views or using only the front-view image, which typically contains the most relevant information needed for most driving tasks. Our annotation results show that both methods yield comparable output quality, so we opt for the front-view image alone to reduce overall complexity.

The second challenge involves integrating temporal information, which is essential for effective planning and decision-making. We also consider two approaches. One straightforward approach is to input several consecutive frames as a sequence, with prompts that indicate the future timestamps. However, we observe that VLMs struggle with temporal continuity and often confuse the ego vehicle’s identity, likely due to limitations in temporal grounding [28, 43]. Instead, we project the ego vehicle’s future trajectory onto a single front-view image, leveraging the camera’s intrinsic and extrinsic parameters along with sensor specifications. We specify in the prompts that the projected trajectory reflects the vehicle’s future path. This cost-effective design allows the VLM to interpret temporal information more reliably than using an image sequence.

Freeform Reasoning Annotation. As a key input to the VLM, a well-designed question is essential for enhancing reasoning capabilities [57] and improving the explainability of the VLM’s responses. In our approach, we focus on the planning task, by designing prompts specifically to obtain reasoning from the VLM. We create two types of questions, beginning with open-ended questions intended to generate free-form, unstructured responses that contain rich, high-

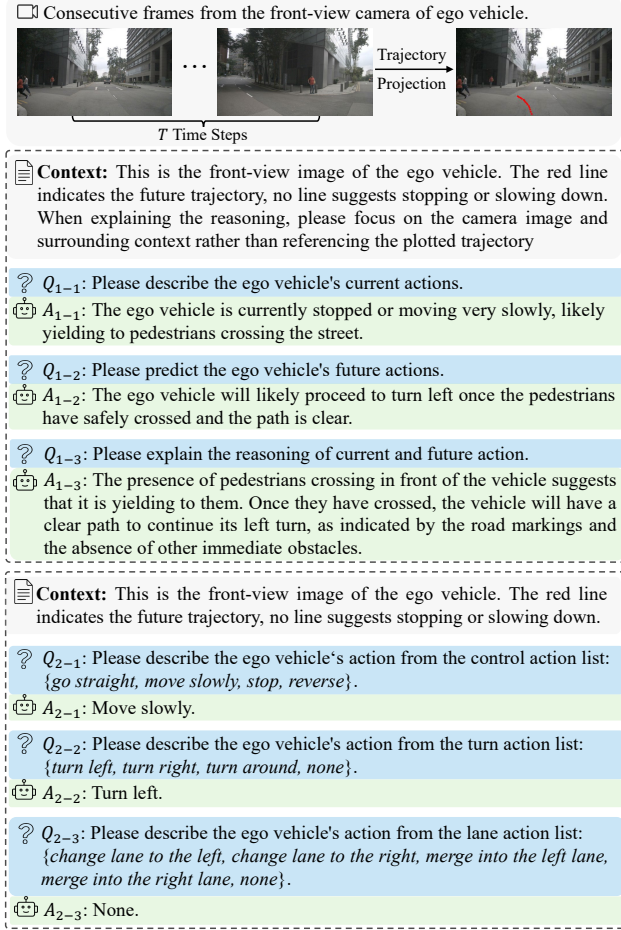


Figure 3. Example annotations from GPT-4o. Given consecutive frames from the front-view camera of the ego vehicle, we project the future trajectory of the vehicle onto the first frame. Using our prompts, we obtain three freeform text responses on the current ego status, anticipated actions, and reasoning, along with three structured action responses.

dimensional language information. We refer to these responses as unstructured reasoning annotations.

To maximize the reasoning capabilities of the VLM, we provide detailed context descriptions as preliminary instructions before posing specific questions. Specifically, the context and questions are defined as follows:

- C_1 : *This is the front-view image of the ego vehicle. The red line indicates the future trajectory, no line suggests stopping or slowing down. When explaining the reasoning, please focus on the camera image and surrounding context rather than referencing the plotted trajectory.*
- Q_{1-1} : *Please describe the ego vehicle's current actions.*
- Q_{1-2} : *Please predict the ego vehicle's future actions.*
- Q_{1-3} : *Please explain the reasoning of current and future action.*

The complete input prompt is defined as $\mathcal{P}_1 = [C_1, Q_1]$, where Q_1 represents the set of questions, $Q_1 = \{Q_{1-1}, Q_{1-2}, Q_{1-3}\}$. These open-ended questions yield free-form text annotations describing the ego vehicle's current status, intended future actions, and the reasoning underlying the VLM's knowledge.

Structured Action Annotation. To examine the flexibility of our method, we define a second type of question in a structured format. Specifically, we create three distinct action sets and prompt the VLM to select answers from these predefined options. This allows us to obtain a single action annotation for each question. Specifically, the context and questions are defined as follows:

- C_2 : *This is the front-view image of the ego vehicle. The red line indicates the future trajectory, no line suggests stopping or slowing down.*
- Q_{2-1} : *Please describe the ego vehicle's action from the control action list: {go straight, move slowly, stop, reverse}.*
- Q_{2-2} : *Please describe the ego vehicle's action from the turn action list: {turn left, turn right, turn around, none}.*
- Q_{2-3} : *Please describe the ego vehicle's action from the lane action list: {change lane to the left, change lane to the right, merge into the left lane, merge into the right lane, none}.*

The complete input prompt is defined as $\mathcal{P}_2 = [C_2, Q_2]$, where Q_2 represents the set of structured action questions, $Q_2 = \{Q_{2-1}, Q_{2-2}, Q_{2-3}\}$. In this way, we can obtain three specific actions from the VLM. Compared to freeform text annotations, one major benefit of structured annotations is that they can be used to supervise an E2E driving model to predict human-interpretable actions, as demonstrated in the experimental results of Sec. 4.

3.2. Auxiliary Heads

Typically, data-driven end-to-end autonomous driving methods [18, 26] focus on summarizing a learnable ego feature f_{ego} to produce planning results, which is essential for generating reliable and accurate planning trajectories. This learnable ego feature aggregates all relevant information about the ego vehicle from upstream modules through different networks. In our approach, we develop auxiliary heads that use this ego feature as input, enabling the model to distill knowledge from the VLM's responses.

Annotation Encoding. Using the Q_1 questions, we obtain three text responses, denoted as $\mathcal{A}_1 = \{\mathcal{A}_c, \mathcal{A}_f, \mathcal{A}_r\}$, which represent descriptions of the current action, future action prediction, and reasoning, respectively. Using the Q_2 questions, we obtain three actions from predefined sets, denoted as $\mathcal{A}_2 = \{\mathcal{A}_{\text{control}}, \mathcal{A}_{\text{turn}}, \mathcal{A}_{\text{lane}}\}$, corresponding to the control action, turn action, and lane action. To convert these annotations into supervisory signals, we apply two distinct approaches to generate two corresponding types of labels, ef-

fectively integrating them into end-to-end autonomous driving pipelines as supervision.

For the freeform text annotations from Q_1 , we utilize an off-the-shelf language model, such as CLIP [45], to convert the text into feature representations. For the structured answers, each action is encoded as a one-hot label. Formally:

$$\begin{aligned} y_1 &= \text{CLIP}(\mathcal{A}_1) \\ y_2 &= \text{One-Hot}(\mathcal{A}_2), \end{aligned} \quad (2)$$

where y_1 and y_2 each have three components: $y_1 = \{y_c, y_f, y_r\}$ and $y_2 = \{y_{\text{control}}, y_{\text{turn}}, y_{\text{lane}}\}$. Here, y_c , y_f , and y_r are feature vectors of size C , where C is the dimension of text embedding, while y_{control} , y_{turn} , and y_{lane} are three one-hot action labels with size N , where $N_{\text{control}} = 4$, $N_{\text{turn}} = 4$ and $N_{\text{lane}} = 5$, respectively.

Text Feature Alignment. Using the three text features $y_1 = \{y_c, y_f, y_r\}$ as supervision, we develop a feature alignment head that takes the ego feature f_{ego} as input. This setup resembles knowledge distillation [16], where the feature alignment head learns to align with the text features provided by the teacher VLM.

In this head, we initialize three learnable text queries, $q_1 = \{q_c, q_f, q_r\}$. Each query interacts with the ego feature f_{ego} via a multi-head cross-attention (MHCA) block, where the text query acts as the attention query q , and the ego feature serves as both the key k and value v , producing updated text queries. These updated queries are then concatenated with the ego feature to form the feature representation for this text head, which is subsequently processed through an MLP layer to produce the final feature alignment output. This process is formulated as:

$$\begin{aligned} q'_1 &= \text{MHCA}(q, k, v) \\ q &= q_1, k = v = f_{\text{ego}}, \\ \hat{f}_1 &= \text{MLP}(q'_1 \oplus f_{\text{ego}}) \end{aligned} \quad (3)$$

where \oplus denotes concatenation, and $\hat{f}_1 = \{\hat{f}_c, \hat{f}_f, \hat{f}_r\}$ represents three output features to be aligned with the corresponding VLM text features. Note that we use three independent MHCA blocks, one for each component, enabling each text query to focus on specific aspects of the ego feature that can be represented in text form.

Inspired by the knowledge distillation approach in DINO [1] that controls the smoothness and sharpness of feature vectors, we adopt a similar strategy to normalize the text and output features with different temperature parameters, producing feature distributions rather than raw feature values as follows:

$$\begin{aligned} P(y_1) &= \frac{\exp(y_1/\tau_t)}{\sum_{k=1}^C \exp(y_1^{(k)}/\tau_t)} \\ P(\hat{f}_1) &= \frac{\exp(\hat{f}_1/\tau_s)}{\sum_{k=1}^C \exp(\hat{f}_1^{(k)}/\tau_s)}, \end{aligned} \quad (4)$$

where τ_t and τ_s are temperature parameters that control the sharpness of these distributions. This adjustment enables better alignment between the output features and supervisory labels, enhancing alignment quality for knowledge distillation. Note that we do not apply the centering operation, as we consider the supervision to be ground truth.

Structured Action Classification. We obtain the structured action labels $y_2 = \{y_{\text{control}}, y_{\text{turn}}, y_{\text{lane}}\}$ from the VLM using question Q_2 . We then construct another action classification head that takes the ego feature f_{ego} as input. Similar to the previous feature alignment stage, we initialize three learnable action queries, q_{control} , q_{turn} , and q_{lane} , which interact with f_{ego} through three MHCA blocks. In this setup, each action query serves as the attention query q , while the ego feature acts as both the key k and value v , producing updated action queries. We then concatenate these updated queries with the ego feature to create the feature representation for the action classification head, passing it through an MLP layer followed by a Softmax function to generate the action predictions. This process is formulated as follows:

$$\begin{aligned} q'_2 &= \text{MHCA}(q, k, v) \\ q &= q_2, k = v = f_{\text{ego}}, \\ \hat{f}_2 &= \text{Softmax}(\text{MLP}(q'_2 \oplus f_{\text{ego}})) \end{aligned} \quad (5)$$

where $\hat{f}_2 = \{\hat{f}_{\text{control}}, \hat{f}_{\text{turn}}, \hat{f}_{\text{lane}}\}$ represents the predicted control action, turn action, and lane action. We use independent MHCA blocks for each action query to produce distinct action labels.

3.3. Auxiliary Loss

We define two parallel auxiliary tasks following the planning module to enable the model to distill knowledge from the VLM, and the overall training loss is defined as a weighted sum of two components:

$$\mathcal{L} = \lambda_1 \mathcal{L}_{\text{align}} + \lambda_2 \mathcal{L}_{\text{action}}, \quad (6)$$

where each component corresponds to a distinct auxiliary text head, providing supervision in the targeted area:

$$\begin{aligned} \mathcal{L}_{\text{align}} &= -P(y_c) \log(P(\hat{f}_c)) - P(y_f) \log(P(\hat{f}_f)) \\ &\quad - P(y_r) \log(P(\hat{f}_r)) \\ \mathcal{L}_{\text{action}} &= - \sum_{i=1}^{N_{\text{control}}} y_{\text{control}}^i \log(\hat{f}_{\text{control}}^i) \\ &\quad - \sum_{i=1}^{N_{\text{turn}}} y_{\text{turn}}^i \log(\hat{f}_{\text{turn}}^i) \\ &\quad - \sum_{i=1}^{N_{\text{lane}}} y_{\text{lane}}^i \log(\hat{f}_{\text{lane}}^i) \end{aligned} \quad (7)$$

For feature alignment, we use cross-entropy loss to align the supervisory and output features, capturing the critical

information conveyed by the text. For the action classification task, we also apply cross-entropy loss to ensure accurate classification.

4. Experiments

4.1. Settings

Baselines. Our proposed method is a general framework compatible with various end-to-end autonomous driving methods. We validate its effectiveness by applying it to two widely recognized open-source methods, UniAD [18] and VAD [26]. Additionally, we compare it with VLP [40], which projects ego vehicle ground-truth labels into text feature space via CLIP [45] for contrastive learning.

Dataset. We use the nuScenes dataset [3] for open-loop planning evaluation. nuScenes is a large-scale autonomous driving dataset featuring 1000 scenes, each with a duration of approximately 20 seconds and annotated at 2Hz. The dataset includes detailed annotations, making it a popular benchmark for end-to-end autonomous driving research.

Evaluation Protocol. We focus on the planning task and use standard metrics such as L2 displacement error and collision rate to evaluate performance.

Implementation Details. We use official codes of the UniAD¹ and VAD², adhering to the hyperparameters specified in their official implementations. For our proposed VLM-AD, we define two auxiliary task heads, each containing an MHCA block with 8 heads and 3 cross-attention layers, and we set 3 text queries for each of Q_1 and Q_2 . During training, we set the temperature parameters $\tau_s = 0.1$ and $\tau_t = 0.04$ to control the sharpness of the features, and we set $\lambda_1 = 1$ and $\lambda_2 = 0.1$ to balance \mathcal{L}_{align} and \mathcal{L}_{action} . All models are trained on 8 NVIDIA H100 GPUs using the PyTorch framework [41]. Complete implementation details, annotation quality analysis, and more experiments are provided in the supplementary material.

4.2. Main Results

Tab. 1 presents the results of applying our proposed VLM-AD to two baselines, UniAD and VAD, as well as comparisons with VLP. Comparing methods ID 0 and 1, we achieve nearly identical planning results using authors’ officially trained checkpoints. For methods IDs 6 and 7, and IDs 12 and 13, we observe some discrepancies between our reproduced results and the reported values, which we attribute to a correction in image configuration in the official codebase³. From the first section of the table, we observe that VLM-AD significantly outperforms UniAD on both average L2 planning error and average collision rate by introducing Q_1 and Q_2 . It also surpasses a state-of-the-art baseline VLP in

both metrics. Regarding VAD, our VLM-AD consistently outperforms both VAD-Base and VAD-Tiny, particularly on the L2 planning error metric, and it achieves superior performance compared to the VLP in VAD-Base. These results demonstrate the effectiveness and advantages of our VLM-AD approach. Additionally, Q_1 yields better results than Q_2 , verifying the value of supervising the driving model through rich reasoning information.

4.3. Ablation Study

Sub-Question Contribution. We further analyze the contributions of each sub-question, Q_{1-1} , Q_{1-2} , and Q_{1-3} , within Q_1 . Each sub-question provides specific text information related to the ego vehicle’s current status, predicted future actions, and reasoning. Tab. 2 presents an ablation study of these three sub-questions. The results indicate that each sub-question positively impacts the overall performance, demonstrating that our designed questions provide valuable information for the planning task. Notably, the reasoning feature contributes the most to reducing the L2 planning error, underscoring its importance in enhancing driving performance.

Feature Alignment Loss. We also study alternative options of feature alignment, including minimizing contrastive learning loss in CLIP [45], MSE loss, KL divergence loss [30], or maximizing negative cosine similarity to align the three features from Q_1 . The results, shown in Tab. 3, indicate that MSE loss performs slightly better than UniAD, by minimizing the Euclidean distance between features, driving outputs toward their mean that causes information loss during training. Both CLIP loss, KL divergence, and cosine similarity outperform UniAD but are inferior to our alignment loss. This underscores the importance of normalizing with different temperatures to balance the smoothness and sharpness of teacher-student features.

Model Design. We investigate alternative design options in our method. First, we use an MLP layer instead of the MHCA block in our structured action classification head. Second, we study different language models, such as T5 [46], MPNet [50] in addition to CLIP for encoding text annotations from Q_1 . From Tab. 4, we observe that achieves slightly worse L2 performance and the same collision rate. Additionally, we observe that both T5 and MPNet outperform UniAD baseline, but slightly worse than CLIP.

Hyperparameter Study. Balancing the losses of different tasks is a critical challenge in multi-task learning. We study the hyperparameters λ_1 and λ_2 in the context of UniAD. The results, shown in Tab. 5, indicate that all three variants outperform UniAD. Among these variants, the performance is the worst when $\lambda_1 = 0.1$ and $\lambda_2 = 1$, as the annotations for Q_1 contain more valuable information compared to the annotations for Q_2 .

¹<https://github.com/OpenDriveLab/UniAD>

²<https://github.com/hustvl/VAD>

³<https://github.com/hustvl/VAD/issues/9>

ID	Method	Q_1	Q_2	L2 (m) ↓				Collision Rate (%) ↓				Ckpt. Source
				1s	2s	3s	Avg.	1s	2s	3s	Avg.	
0	UniAD [18]			0.48	0.96	1.65	1.03	<u>0.05</u>	0.17	0.71	0.31	Official
1	UniAD*			0.46	0.96	1.67	1.03	0.11	0.22	0.74	0.36	Reproduced
2	VLP [40]			0.43	0.86	1.47	0.92	0.03	0.15	<u>0.48</u>	<u>0.22</u>	Official
3	VLM-AD	✓		<u>0.40</u>	<u>0.83</u>	<u>1.44</u>	<u>0.89</u>	<u>0.05</u>	0.11	0.56	0.24	-
4	VLM-AD		✓	0.41	0.87	1.46	0.91	0.06	<u>0.13</u>	0.68	0.29	-
5	VLM-AD	✓	✓	0.39	0.82	1.43	0.88	<u>0.05</u>	0.11	0.43	0.19	-
6	VAD-Base [26]			0.41	0.70	1.06	0.72	0.04	0.43	1.15	0.54	Official
7	VAD-Base [#]			0.33	0.59	0.94	0.62	0.19	0.30	0.53	0.34	Reproduced
8	VLP [40]			<u>0.26</u>	<u>0.47</u>	0.78	0.50	<u>0.12</u>	<u>0.17</u>	<u>0.42</u>	0.23	Official
9	VLM-AD	✓		0.24	0.48	<u>0.76</u>	<u>0.49</u>	<u>0.12</u>	0.16	0.41	0.23	-
10	VLM-AD		✓	0.30	0.50	0.82	0.54	0.16	0.24	0.43	<u>0.28</u>	-
11	VLM-AD	✓	✓	0.24	0.46	0.75	0.48	<u>0.12</u>	<u>0.17</u>	0.41	0.23	-
12	VAD-Tiny [26]			0.46	0.76	1.12	0.78	0.21	0.35	0.58	0.38	Official
13	VAD-Tiny [#]			0.35	0.62	0.96	0.64	0.12	0.19	0.44	0.25	Reproduced
14	VLM-AD	✓		0.30	0.54	<u>0.82</u>	0.55	0.08	0.15	0.38	0.20	-
15	VLM-AD		✓	<u>0.31</u>	<u>0.55</u>	0.88	<u>0.58</u>	<u>0.10</u>	<u>0.18</u>	<u>0.41</u>	0.23	-
16	VLM-AD	✓	✓	0.30	0.54	0.80	0.55	0.11	0.15	0.38	<u>0.21</u>	-

Table 1. Planning results of our VLM-AD method and baselines. The best is in bold and the second best is underlined. VLM-AD consistently outperforms the baselines, with the reasoning-focused Q_1 contributing the most significant improvements.

Method	Q_{1-1}	Q_{1-2}	Q_{1-3}	Q_2	L2 (m) ↓				Collision Rate (%) ↓			
					1s	2s	3s	Avg.	1s	2s	3s	Avg.
UniAD					0.48	0.96	1.65	1.03	<u>0.05</u>	0.17	0.71	0.31
VLM-AD	✓	✓			<u>0.41</u>	0.87	1.53	0.94	0.08	0.17	0.61	0.29
VLM-AD	✓		✓		<u>0.41</u>	<u>0.84</u>	1.44	<u>0.90</u>	<u>0.05</u>	0.11	0.48	0.21
VLM-AD		✓	✓		0.42	0.87	<u>1.49</u>	0.93	0.03	<u>0.14</u>	<u>0.51</u>	<u>0.23</u>
VLM-AD	✓	✓	✓		0.40	0.83	1.44	0.89	<u>0.05</u>	0.11	0.56	0.24

Table 2. Ablation study on the contributions of Q_{1-1} , Q_{1-2} and Q_{1-3} . The best is in bold and the second best is underlined.

Method	Variant	Planning Results	
		Avg. L2 ↓	Avg. Col ↓
UniAD	-	1.03	0.31
VLM-AD	CLIP	0.94	<u>0.26</u>
VLM-AD	MSE	0.99	0.30
VLM-AD	KL	<u>0.92</u>	<u>0.26</u>
VLM-AD	CosSim	0.96	0.28
VLM-AD	Align	0.89	0.24

Table 3. Results of different variants of VLM-KD. CLIP indicates the use of the contrastive learning loss defined in [45] to align the text features of Q_1 . MSE represents the use of MSE loss for feature alignment, KL represents KL divergence, and CosSim indicates cosine similarity for aligning features. Align refers to the alignment loss defined in our method.

Method	Variant	Planning Results	
		Avg. L2 ↓	Avg. Col ↓
UniAD	-	1.03	0.31
VLM-AD	MLP	0.94	0.29
VLM-AD	MHCA	0.91	0.29
VLM-AD	T5	0.94	0.29
VLM-AD	MPNet	0.91	0.26
VLM-AD	CLIP	0.89	0.24

Table 4. Results of different designs for VLM-KD. MLP indicates that an MLP layer is used to replace the MHCA block for Q_2 . T5 and MPNet indicate the use of different language models to convert reasoning annotations from Q_1 into reasoning features that serve as supervision labels.



Figure 4. Qualitative comparison between UniAD and our method. The yellow arrow highlights areas where VLM-AD outperforms UniAD. The red box indicates the failure planning command from UniAD, and the purple box represents the predicted three action outputs from our VLM-AD auxiliary text head.

Method	Variant	Planning Results	
		Avg. L2 ↓	Avg. Col ↓
UniAD	-	1.03	0.31
VLM-AD	$\lambda_1 = 1, \lambda_2 = 1$	<u>0.90</u>	<u>0.26</u>
VLM-AD	$\lambda_1 = 0.1, \lambda_2 = 1$	0.92	0.29
VLM-AD	$\lambda_1 = 1, \lambda_2 = 0.1$	0.88	0.19

Table 5. Results of using different hyperparameters of λ_1 and λ_2 to control the weights of \mathcal{L}_{align} and \mathcal{L}_{action} .

4.4. Visualizations

We provide four visualization examples from the nuScenes dataset, as shown in Fig. 4, to demonstrate the effectiveness of our proposed method. In the first, third, and last row cases, UniAD produces planning trajectories that are winding and lack smoothness, whereas our method gener-

ates smoother trajectories that accurately follow the road. Additionally, in the second, third, and last row cases, the commands calculated by the baseline incorrectly suggest a turning intention, while the ego vehicles in these scenarios are actually moving straight. Our action text head correctly outputs the control action “go straight” for all three cases, not only verifying the effectiveness of VLM supervision but also offering interpretability of the model’s decisions.

5. Conclusion

In this work, we presented VLM-AD, a novel approach to enhancing end-to-end autonomous driving models by leveraging vision-language models (VLMs) as auxiliary teachers. By integrating VLM-based annotations through targeted questions that include unstructured reasoning text and structured action labels, we enriched the training pro-

cess with additional reasoning and action supervision. Our method demonstrated significant improvements in planning accuracy and reduced collision rates on the nuScenes dataset, and offered interpretability in its output trajectories through action predictions. Importantly, VLM-AD does not require VLMs during inference, making it plug-and-play for real-world deployment without additional inference costs.

References

- [1] Emerging properties in self-supervised vision transformers. In *ICCV*, pages 9650–9660, 2021. 5
- [2] Josh Achiam, Steven Adler, Sandhini Agarwal, Lama Ahmad, Ilge Akkaya, Florencia Leoni Aleman, Diogo Almeida, Janko Altenschmidt, Sam Altman, Shyamal Anadkat, et al. Gpt-4 technical report. *arXiv preprint arXiv:2303.08774*, 2023. 3
- [3] Holger Caesar, Varun Bankiti, Alex H Lang, Sourabh Vora, Venice Erin Liong, Qiang Xu, Anush Krishnan, Yu Pan, Giancarlo Baldan, and Oscar Beijbom. nuscenes: A multimodal dataset for autonomous driving. In *CVPR*, pages 11621–11631, 2020. 2, 6
- [4] Long Chen, Oleg Sinavski, Jan Hünermann, Alice Karnsund, Andrew James Willmott, Danny Birch, Daniel Maund, and Jamie Shotton. Driving with llms: Fusing object-level vector modality for explainable autonomous driving. In *ICRA*, pages 14093–14100, 2024. 1, 2
- [5] Li Chen, Penghao Wu, Kashyap Chitta, Bernhard Jaeger, Andreas Geiger, and Hongyang Li. End-to-end autonomous driving: Challenges and frontiers. *IEEE TPAMI*, 2024. 1
- [6] Shaoyu Chen, Bo Jiang, Hao Gao, Bencheng Liao, Qing Xu, Qian Zhang, Chang Huang, Wenyu Liu, and Xinggang Wang. Vadv2: End-to-end vectorized autonomous driving via probabilistic planning. *arXiv preprint arXiv:2402.13243*, 2024. 2
- [7] Pranav Singh Chib and Pravendra Singh. Recent advancements in end-to-end autonomous driving using deep learning: A survey. *IEEE TIV*, 2023. 1
- [8] Kashyap Chitta, Aditya Prakash, and Andreas Geiger. Neat: Neural attention fields for end-to-end autonomous driving. In *ICCV*, pages 15793–15803, 2021. 2
- [9] Kashyap Chitta, Aditya Prakash, Bernhard Jaeger, Zehao Yu, Katrin Renz, and Andreas Geiger. Transfuser: Imitation with transformer-based sensor fusion for autonomous driving. *IEEE TPAMI*, 45(11):12878–12895, 2022. 2
- [10] Tushar Choudhary, Vikrant Dewangan, Shivam Chandhok, Shubham Priyadarshan, Anushka Jain, Arun K Singh, Siddharth Srivastava, Krishna Murthy Jatavallabhula, and K Madhava Krishna. Talk2bev: Language-enhanced bird’s-eye view maps for autonomous driving. In *ICRA*, pages 16345–16352, 2024. 2
- [11] Can Cui, Yunsheng Ma, Xu Cao, Wenqian Ye, and Ziran Wang. Receive, reason, and react: Drive as you say, with large language models in autonomous vehicles. *IEEE ITSM*, 2024. 2
- [12] Jacob Devlin. Bert: Pre-training of deep bidirectional transformers for language understanding. *arXiv preprint arXiv:1810.04805*, 2018. 1
- [13] Kairui Ding, Boyuan Chen, Yuchen Su, Huan-ang Gao, Bu Jin, Chonghao Sima, Wuqiang Zhang, Xiaohui Li, Paul Barsch, Hongyang Li, et al. Hint-ad: Holistically aligned interpretability in end-to-end autonomous driving. *arXiv preprint arXiv:2409.06702*, 2024. 1
- [14] Alexey Dosovitskiy, German Ros, Felipe Codevilla, Antonio Lopez, and Vladlen Koltun. Carla: An open urban driving simulator. In *CoRL*, pages 1–16, 2017. 2

- [15] Daocheng Fu, Xin Li, Licheng Wen, Min Dou, Pinlong Cai, Botian Shi, and Yu Qiao. Drive like a human: Rethinking autonomous driving with large language models. In *WACV*, pages 910–919, 2024. [2](#)
- [16] Geoffrey Hinton. Distilling the knowledge in a neural network. *arXiv preprint arXiv:1503.02531*, 2015. [5](#)
- [17] Shengchao Hu, Li Chen, Penghao Wu, Hongyang Li, Junchi Yan, and Dacheng Tao. St-p3: End-to-end vision-based autonomous driving via spatial-temporal feature learning. In *ECCV*, pages 533–549, 2022. [1](#), [2](#)
- [18] Yihan Hu, Jiazhi Yang, Li Chen, Keyu Li, Chonghao Sima, Xizhou Zhu, Siqi Chai, Senyao Du, Tianwei Lin, Wenhai Wang, et al. Planning-oriented autonomous driving. In *CVPR*, pages 17853–17862, 2023. [1](#), [2](#), [4](#), [6](#), [7](#), [12](#)
- [19] Zhiyu Huang, Chen Lv, Yang Xing, and Jingda Wu. Multi-modal sensor fusion-based deep neural network for end-to-end autonomous driving with scene understanding. *IEEE Sensors Journal*, 21(10):11781–11790, 2020. [2](#)
- [20] Jyh-Jing Hwang, Runsheng Xu, Hubert Lin, Wei-Chih Hung, Jingwei Ji, Kristy Choi, Di Huang, Tong He, Paul Covington, Benjamin Sapp, et al. Emma: End-to-end multimodal model for autonomous driving. *arXiv preprint arXiv:2410.23262*, 2024. [1](#)
- [21] Yuichi Inoue, Yuki Yada, Kotaro Tanahashi, and Yu Yamaguchi. Nuscenes-mqa: Integrated evaluation of captions and qa for autonomous driving datasets using markup annotations. In *WACV*, pages 930–938, 2024. [2](#)
- [22] Keishi Ishihara, Anssi Kanervisto, Jun Miura, and Ville Hautamaki. Multi-task learning with attention for end-to-end autonomous driving. In *CVPR*, pages 2902–2911, 2021. [3](#)
- [23] Bernhard Jaeger, Kashyap Chitta, and Andreas Geiger. Hidden biases of end-to-end driving models. In *ICCV*, pages 8240–8249, 2023. [2](#)
- [24] Fan Jia, Weixin Mao, Yingfei Liu, Yucheng Zhao, Yuqing Wen, Chi Zhang, Xiangyu Zhang, and Tiancai Wang. Driver-i: A general world model for autonomous driving. *arXiv preprint arXiv:2311.13549*, 2023. [2](#)
- [25] Xiaosong Jia, Penghao Wu, Li Chen, Jiangwei Xie, Conghui He, Junchi Yan, and Hongyang Li. Think twice before driving: Towards scalable decoders for end-to-end autonomous driving. In *CVPR*, pages 21983–21994, 2023. [2](#)
- [26] Bo Jiang, Shaoyu Chen, Qing Xu, Bencheng Liao, Jiajie Chen, Helong Zhou, Qian Zhang, Wenyu Liu, Chang Huang, and Xinggang Wang. Vad: Vectorized scene representation for efficient autonomous driving. In *ICCV*, pages 8340–8350, 2023. [1](#), [2](#), [4](#), [6](#), [7](#), [12](#)
- [27] Bu Jin, Xinyu Liu, Yupeng Zheng, Pengfei Li, Hao Zhao, Tong Zhang, Yuhang Zheng, Guyue Zhou, and Jingjing Liu. Adapt: Action-aware driving caption transformer. In *ICRA*, pages 7554–7561, 2023. [1](#), [2](#)
- [28] Ilker Kesen, Andrea Pedrotti, Mustafa Dogan, Michele Cafagna, Emre Can Acikgoz, Letitia Parcalabescu, Iacer Calixto, Anette Frank, Albert Gatt, Aykut Erdem, et al. Vilma: A zero-shot benchmark for linguistic and temporal grounding in video-language models. *arXiv preprint arXiv:2311.07022*, 2023. [3](#)
- [29] Ali Keysan, Andreas Look, Eitan Kosman, Gonca Gürsun, Jörg Wagner, Yu Yao, and Barbara Rakitsch. Can you text what is happening? integrating pre-trained language encoders into trajectory prediction models for autonomous driving. *arXiv preprint arXiv:2309.05282*, 2023. [2](#)
- [30] Solomon Kullback. *Information theory and statistics*. Courier Corporation, 1997. [6](#)
- [31] Junnan Li, Dongxu Li, Caiming Xiong, and Steven Hoi. Blip: Bootstrapping language-image pre-training for unified vision-language understanding and generation. In *ICML*, pages 12888–12900, 2022. [1](#)
- [32] Junnan Li, Dongxu Li, Silvio Savarese, and Steven Hoi. Blip-2: Bootstrapping language-image pre-training with frozen image encoders and large language models. In *ICML*, pages 19730–19742, 2023. [1](#)
- [33] Zhihao Li, Toshiyuki Motoyoshi, Kazuma Sasaki, Tetsuya Ogata, and Shigeki Sugano. Rethinking self-driving: Multi-task knowledge for better generalization and accident explanation ability. *arXiv preprint arXiv:1809.11100*, 2018. [2](#)
- [34] Zhiqi Li, Wenhai Wang, Hongyang Li, Enze Xie, Chonghao Sima, Tong Lu, Yu Qiao, and Jifeng Dai. Bevformer: Learning bird’s-eye-view representation from multi-camera images via spatiotemporal transformers. In *ECCV*, pages 1–18, 2022. [12](#)
- [35] Zhiqi Li, Zhiding Yu, Shiyi Lan, Jiahan Li, Jan Kautz, Tong Lu, and Jose M Alvarez. Is ego status all you need for open-loop end-to-end autonomous driving? In *CVPR*, pages 14864–14873, 2024. [2](#)
- [36] Haotian Liu, Chunyuan Li, Qingyang Wu, and Yong Jae Lee. Visual instruction tuning. In *Advances in neural information processing systems*, pages 34892–34916, 2024. [1](#)
- [37] I Loshchilov. Decoupled weight decay regularization. *arXiv preprint arXiv:1711.05101*, 2017. [12](#)
- [38] Ilya Loshchilov and Frank Hutter. Sgdr: Stochastic gradient descent with warm restarts. *arXiv preprint arXiv:1608.03983*, 2016. [12](#)
- [39] Jiageng Mao, Yuxi Qian, Junjie Ye, Hang Zhao, and Yue Wang. Gpt-driver: Learning to drive with gpt. In *NeurIPS Workshop*, 2023. [1](#), [2](#)
- [40] Chenbin Pan, Burhaneddin Yaman, Tommaso Nesti, Abhirup Mallik, Alessandro G Allievi, Senem Velipasalar, and Liu Ren. Vlp: Vision language planning for autonomous driving. In *CVPR*, pages 14760–14769, 2024. [1](#), [2](#), [6](#), [7](#)
- [41] Adam Paszke, Sam Gross, Francisco Massa, Adam Lerer, James Bradbury, Gregory Chanan, Trevor Killeen, Zeming Lin, Natalia Gimelshein, Luca Antiga, et al. Pytorch: An imperative style, high-performance deep learning library. In *NeurIPS*, 2019. [6](#)
- [42] Tianwen Qian, Jingjing Chen, Linhai Zhuo, Yang Jiao, and Yu-Gang Jiang. Nuscenes-qa: A multi-modal visual question answering benchmark for autonomous driving scenario. In *AAAI*, pages 4542–4550, 2024. [2](#)
- [43] Yifu Qiu, Zheng Zhao, Yftah Ziser, Anna Korhonen, Edoardo M Ponti, and Shay B Cohen. Are large language models temporally grounded? *arXiv preprint arXiv:2311.08398*, 2023. [3](#)
- [44] Alec Radford. Improving language understanding by generative pre-training. 2018. [1](#)

- [45] Alec Radford, Jong Wook Kim, Chris Hallacy, Aditya Ramesh, Gabriel Goh, Sandhini Agarwal, Girish Sastry, Amanda Askell, Pamela Mishkin, Jack Clark, et al. Learning transferable visual models from natural language supervision. In *ICML*, pages 8748–8763, 2021. [1](#), [5](#), [6](#), [7](#), [12](#)
- [46] Colin Raffel, Noam Shazeer, Adam Roberts, Katherine Lee, Sharan Narang, Michael Matena, Yanqi Zhou, Wei Li, and Peter J Liu. Exploring the limits of transfer learning with a unified text-to-text transformer. *JMLR*, 21(140):1–67, 2020. [6](#), [12](#)
- [47] Hao Shao, Letian Wang, Ruobing Chen, Hongsheng Li, and Yu Liu. Safety-enhanced autonomous driving using interpretable sensor fusion transformer. In *CoRL*, pages 726–737, 2023. [2](#)
- [48] Hao Shao, Letian Wang, Ruobing Chen, Steven L Waslander, Hongsheng Li, and Yu Liu. Reasonnet: End-to-end driving with temporal and global reasoning. In *CVPR*, pages 13723–13733, 2023. [2](#)
- [49] Chonghao Sima, Katrin Renz, Kashyap Chitta, Li Chen, Hanxue Zhang, Chengen Xie, Ping Luo, Andreas Geiger, and Hongyang Li. Drivelm: Driving with graph visual question answering. In *ECCV*, 2024. [2](#)
- [50] Kaitao Song, Xu Tan, Tao Qin, Jianfeng Lu, and Tie-Yan Liu. Mpnnet: Masked and permuted pre-training for language understanding. In *NeurIPS*, pages 16857–16867, 2020. [6](#), [12](#)
- [51] Xiaoyu Tian, Junru Gu, Bailin Li, Yicheng Liu, Chenxu Hu, Yang Wang, Kun Zhan, Peng Jia, Xianpeng Lang, and Hang Zhao. Drivevlm: The convergence of autonomous driving and large vision-language models. *arXiv preprint arXiv:2402.12289*, 2024. [1](#), [2](#)
- [52] Hugo Touvron, Thibaut Lavril, Gautier Izacard, Xavier Martinet, Marie-Anne Lachaux, Timothée Lacroix, Baptiste Rozière, Naman Goyal, Eric Hambro, Faisal Azhar, et al. Llama: Open and efficient foundation language models. *arXiv preprint arXiv:2302.13971*, 2023. [1](#)
- [53] Pengqin Wang, Meixin Zhu, Hongliang Lu, Hui Zhong, Xiananda Chen, Shaojie Shen, Xuesong Wang, and Yinhai Wang. Bevqpt: Generative pre-trained large model for autonomous driving prediction, decision-making, and planning. *arXiv preprint arXiv:2310.10357*, 2023. [2](#)
- [54] Shihao Wang, Zhiding Yu, Xiaohui Jiang, Shiyi Lan, Min Shi, Nadine Chang, Jan Kautz, Ying Li, and Jose M Alvarez. Omnidrive: A holistic llm-agent framework for autonomous driving with 3d perception, reasoning and planning. *arXiv preprint arXiv:2405.01533*, 2024. [1](#)
- [55] Wenhai Wang, Jiangwei Xie, ChuanYang Hu, Haoming Zou, Jianan Fan, Wenwen Tong, Yang Wen, Silei Wu, Hanming Deng, Zhiqi Li, et al. Drivelm: Aligning multi-modal large language models with behavioral planning states for autonomous driving. *arXiv preprint arXiv:2312.09245*, 2023. [1](#), [2](#)
- [56] Xiaofeng Wang, Zheng Zhu, Guan Huang, Xinze Chen, Jiagan Zhu, and Jiwen Lu. Drivedreamer: Towards real-world-driven world models for autonomous driving. *arXiv preprint arXiv:2309.09777*, 2023. [2](#)
- [57] Jason Wei, Xuezhi Wang, Dale Schuurmans, Maarten Bosma, Fei Xia, Ed Chi, Quoc V Le, Denny Zhou, et al. Chain-of-thought prompting elicits reasoning in large language models. In *NeurIPS*, pages 24824–24837, 2022. [3](#)
- [58] Xinshuo Weng, Boris Ivanovic, Yan Wang, Yue Wang, and Marco Pavone. Para-drive: Parallelized architecture for real-time autonomous driving. In *CVPR*, pages 15449–15458, 2024. [2](#)
- [59] Penghao Wu, Xiaosong Jia, Li Chen, Junchi Yan, Hongyang Li, and Yu Qiao. Trajectory-guided control prediction for end-to-end autonomous driving: A simple yet strong baseline. In *NeurIPS*, pages 6119–6132, 2022. [3](#)
- [60] Huazhe Xu, Yang Gao, Fisher Yu, and Trevor Darrell. End-to-end learning of driving models from large-scale video datasets. In *CVPR*, pages 2174–2182, 2017. [2](#)
- [61] Zhenhua Xu, Yujia Zhang, Enze Xie, Zhen Zhao, Yong Guo, Kwan-Yee K Wong, Zhenguo Li, and Hengshuang Zhao. Drivegpt4: Interpretable end-to-end autonomous driving via large language model. *IEEE RA-L*, 2024. [1](#), [2](#)
- [62] Jiang-Tian Zhai, Ze Feng, Jinhao Du, Yongqiang Mao, Jiang-Jiang Liu, Zichang Tan, Yifu Zhang, Xiaoqing Ye, and Jingdong Wang. Rethinking the open-loop evaluation of end-to-end autonomous driving in nuscenes. *arXiv preprint arXiv:2305.10430*, 2023. [2](#)
- [63] Jimuyang Zhang, Zanming Huang, and Eshed Ohn-Bar. Coaching a teachable student. In *CVPR*, pages 7805–7815, 2023. [2](#)
- [64] Guosheng Zhao, Xiaofeng Wang, Zheng Zhu, Xinze Chen, Guan Huang, Xiaoyi Bao, and Xingang Wang. Drivedreamer-2: Llm-enhanced world models for diverse driving video generation. *arXiv preprint arXiv:2403.06845*, 2024. [2](#)

A. Implementation Details

When integrating our proposed VLM-AD method into UniAD [18], we follow the joint training protocol defined in UniAD. In the first stage, we initialize the model using BEVFormer [34] weights and train the perception and mapping tasks for 6 epochs. In the second stage, we freeze the image backbone and BEV encoder and perform end-to-end training using our proposed VLM-AD approach for 20 epochs. The model is trained using an initial learning rate of 2×10^{-4} , a learning rate multiplier of 0.1, and the AdamW optimizer [37] with a weight decay of 0.01.

When integrating our proposed VLM-AD method into VAD [26], we adopt the same hyperparameters as in their original implementation. The model is trained using the AdamW optimizer [37] and a cosine annealing scheduler [38], with a weight decay of 0.01 and an initial learning rate of 2×10^{-4} .

To encode freeform annotations into text features, we use the pre-trained CLIP-ViT-B/32 [45] model with a dimension of 512. Additionally, we experiment with other text encoders such as T5-base [46] and MPNet-base [50], both encoding freeform annotations into text features with a dimension of 768, as described in Sec. 4.3.

B. VLM Annotation

In this section, we provide a comprehensive analysis of our VLM annotations, including visual input format comparisons, annotation statistics, as well as the annotation quality, including representative successful and failure examples.

B.1. Visual Input

While we use a front-view image (as shown in Fig. 5) as the visual input to the VLM, we also experiment with other alternatives described in Sec. 3, including six images covering the full 360-degree surroundings of the ego vehicle (Fig. 6) and a sequence of consecutive front-view images (Fig. 7). Compared to the first alternative that uses the full 360-degree surrounding as input, our approach yields similar annotations from the VLM while significantly reducing the computational cost by processing a much smaller input image. The second alternative, which utilizes consecutive front-view images, often results in incorrect annotations, such as misidentifying the current action status and failing to detect a left-turn action. This is due to the challenge VLMs face in understanding temporal dynamics, especially from ego-centric visual signals. Furthermore, using consecutive images increases the annotation time by approximately 80% compared to our approach.

B.2. Annotation Statistics

We annotate the training set of the nuScenes dataset, which consists of 700 scenes and 28,130 frames. Following the



A_c : The ego vehicle is currently moving forward at a moderate speed.
 A_f : The ego vehicle is likely to continue moving forward and follow the curve of the road to the left.
 A_r : The road ahead is clear with no visible obstacles or traffic, allowing the vehicle to maintain its current speed and direction. The environment suggests a low-traffic area, and the road's curve indicates the vehicle will naturally follow it to the left.
 $A_{control}$: move slowly
 A_{turn} : turn left
 A_{lane} : none

Figure 5. An annotation example of our approach, by projecting the ego vehicle’s future trajectory onto the front-view image.



Context: This is an overview image covering the entire 360-degree surroundings of the ego vehicle. The red line indicates the future trajectory, no line suggests stopping or slowing down. When explaining the reasoning, please focus on the camera image and surrounding context rather than referencing the plotted trajectory.
 A_c : The ego vehicle is moving forward on a clear road.
 A_f : The ego vehicle is likely to turn left.
 A_r : The road is clear with no visible obstacles, and the surroundings suggest a typical urban environment. The presence of lane markings and the absence of traffic support the likelihood of a left turn.
 $A_{control}$: move slowly
 A_{turn} : turn left
 A_{lane} : none

Figure 6. An annotation example using all 6 images, with ego vehicle’s future trajectory projected onto the front-view image.

methodology described in Sec. 3, we set $T = 6$ to project the ego vehicle’s future trajectory onto the front-view image. Consistent with UniAD [18], we exclude samples lacking sufficient input data, resulting in a total of 28,032 annotated samples.

For freeform reasoning annotations using Q_1 , we cal-



Context: These are 7 consecutive front-view images of the ego vehicle. The first image represents the current time step, while the following 6 images represent the next 6 future time steps.

A_c : The ego vehicle is **moving forward along a straight path**.

A_f : The ego vehicle will continue to move forward, approaching the speed bump and gate visible in the images.

A_r : The sequence of images shows the vehicle gradually moving closer to the speed bump and gate, indicating forward motion. The road markings and alignment suggest the vehicle is maintaining a straight path. The environment appears controlled, with clear lane markings and a speed limit sign, guiding the vehicle's movement.

A_{control} : go straight

A_{turn} : none

A_{lane} : none

Figure 7. An annotation example using 7 consecutive front-view images as the visual input, which results in incorrect annotations.

Word Length	Annotation \mathcal{A}_1		
	\mathcal{A}_c	\mathcal{A}_f	\mathcal{A}_r
Max	29	41	93
Min	6	7	13
Mean	11.30	15.34	35.85

Table 6. Statistics of freeform text annotation \mathcal{A}_1 from Q_1 .

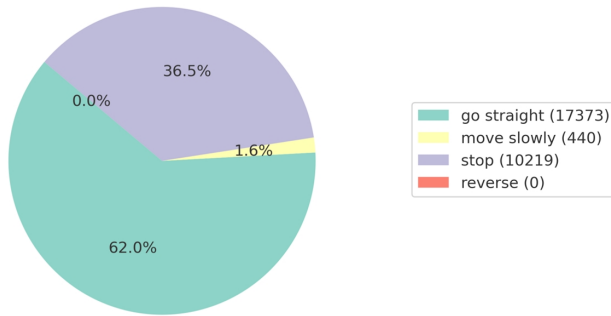


Figure 8. Control action distribution.

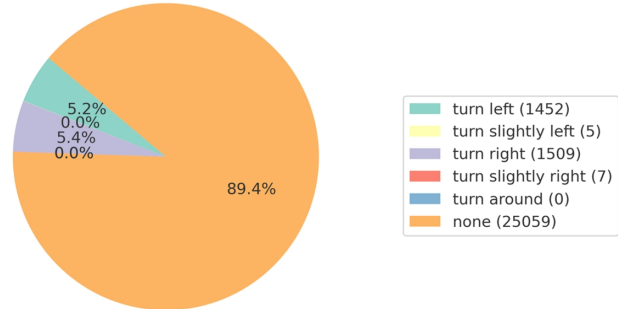


Figure 9. Turn action distribution.

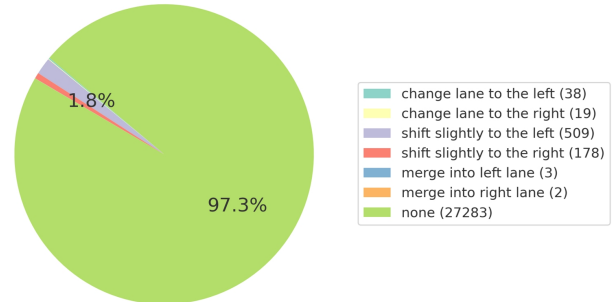


Figure 10. Lane action distribution.

culate the word length of responses for each sub-question (Q_{1-1} , Q_{1-2} , and Q_{1-3}). The statistics are presented in Tab. 6, in which the average response length of \mathcal{A}_r is the longest, as this sub-question focuses on detailed reasoning information.

For structured action annotations using Q_2 , we analyze the distribution of three types of actions. The results are shown in Fig. 8, Fig. 9 and Fig. 10. Approximately 62% of frames are labeled as “go straight”, 89.4% as “no turn action”, and 97.3% as “no lane action”. Notably, no frames are labeled with “reverse” or “turn around”, and only a very small number of frames are labeled as “merge into left lane” or “merge into right lane”. These statistics suggest that the nuScenes dataset has limited diversity in driving actions.

An interesting observation is that the VLM occasionally outputs actions not included in our predefined action list. For example, it generates actions such as “turn slightly left”,

“turn slightly right”, “shift slightly to the left”, and “shift slightly to the right”. In our work, we merge these outputs into our predefined one-hot categories: “turn slightly left” is merged with “turn left”, “turn slightly right” with “turn right”, “shift slightly to the left” with “change lane to the left”, and “shift slightly to the right” with “change lane to the right”. This highlights the advantage of using structured annotations, as they help mitigate hallucinations by constraining VLM outputs to predefined categories.

B.3. Annotation Quality

To validate the annotation quality from the VLM, we make a questionnaire with a random sample of 50 cases for eval-

uation. For each case, participants are provided with the front-view image of the ego vehicle, projected with its future trajectory, along with the corresponding VLM annotations of Q_1 and Q_2 .

Participants are then asked to score each response. For freeform reasoning annotations, we set a scoring criterion on a 1 to 5 scale as follows:

- **5 Points:** Highly Consistent.
 - The text description perfectly matches the image.
 - Key elements of the image (e.g., vehicle state, action, reasoning) are accurately described.
 - The text is clear, concise, and complete, with no unnecessary details or contradictions.
- **4 Points:** Mostly Consistent.
 - The text description mostly aligns with the image, with minor inaccuracies or omissions.
 - Key elements are described but may lack some secondary details.
 - Alternatively, the text may contain minor redundancies or slightly unrelated details that don't impact the overall match.
- **3 Points:** Partially Consistent.
 - The text description partially matches the image but has notable inaccuracies or missing details.
 - Important aspects of the image (e.g., vehicle speed, road conditions) may be under- or misrepresented.
 - There could be some conflicting or vague statements.
- **2 Points:** Mostly Inconsistent.
 - The text description is largely inconsistent with the image but contains a small amount of relevant information.
 - The description fails to capture critical details of the image or includes noticeable inaccuracies.
 - Logical errors or contradictions in the text are present.
- **1 Point:** Completely Inconsistent.
 - The text description does not match the image at all.
 - The text is entirely irrelevant or contradicts the image in significant ways.
 - Misleading information that severely detracts from interpretability.

For structured action annotations, we ask the participants to score True or False for each action.

We evaluated the results from 5 participants, as summarized in Tab. 7. The scores validate the overall annotation quality. Specifically, the annotation \mathcal{A}_f , which predicts future actions, received the highest score, while the annotation \mathcal{A}_r , which describes reasoning, received the lowest. Additionally, for action annotations, the accuracy for all three action types is 90% or higher, with the lane action achieving the highest accuracy at 96%.

Participant	Average Score (1-5)			Accuracy (%)		
	\mathcal{A}_c	\mathcal{A}_f	\mathcal{A}_r	$\mathcal{A}_{\text{control}}$	$\mathcal{A}_{\text{turn}}$	$\mathcal{A}_{\text{lane}}$
1	4.58	4.66	4.26	0.88	0.96	0.98
2	4.34	4.26	4.34	0.86	0.92	0.94
3	4.86	4.66	4.54	0.98	0.84	0.96
4	4.12	4.34	4.40	0.80	0.84	0.94
5	4.50	4.62	4.56	0.98	0.96	0.98
Average	4.48	4.51	4.42	0.90	0.90	0.96
Std	0.28	0.19	0.13	0.08	0.06	0.02

Table 7. Summary of questionnaire results from 5 participants evaluating both freeform annotations and structured action labels. Std represents the standard deviation among the participants.

B.4. Successful Annotation Examples

We present three examples to demonstrate the quality of VLM annotations, as shown in Fig. 11, Fig. 12, and Fig. 13.

In Fig. 11, the VLM accurately identifies the red traffic light and suggests a stop action at the intersection. It also predicts a reasonable future action and clearly explains the rationale behind its decisions.

In Fig. 12, a white van is observed ahead of the ego vehicle but in the opposite lane. The VLM correctly assesses that the van will not affect the ego vehicle's movement and outputs appropriate driving actions.

In Fig. 13, the ego vehicle is stopped at an intersection on a rainy day. Despite low visibility, the VLM successfully identifies the red traffic light and predicts the future movement based on the traffic light's status.

B.5. Imperfect Annotation Examples

We also present three annotation failure cases, illustrated in Fig. 14, Fig. 15, and Fig. 16.

In Fig. 14, the VLM accurately recognizes that the traffic light is green and predicts a future right-turn action from its reasoning annotation. However, it incorrectly outputs a left-turn action from the action annotation. Since we query Q_1 and Q_2 separately, the response to Q_1 does not influence Q_2 . One potential solution is to introduce additional prompts to establish a progressive questioning process toward more accurate action annotations.



A_c : The ego vehicle is currently stopped or moving very slowly at the intersection.
 A_f : The ego vehicle will remain stopped until the traffic light turns green and the pedestrian has safely crossed the street.
 A_r : The red traffic light and the pedestrian crossing in front of the vehicle indicate that it is necessary for the ego vehicle to stop to ensure safety and compliance with traffic rules.
 $A_{control}$: stop
 A_{turn} : none
 A_{lane} : none

Figure 11. A successful annotation example where the red traffic light is correctly identified, and the annotations are complete and informative.



A_c : The ego vehicle is currently stopped or moving very slowly.
 A_f : The ego vehicle will likely remain stopped until the traffic light turns green, at which point it may proceed cautiously.
 A_r : The red traffic light indicates that the vehicle should stop to comply with traffic regulations. The wet road conditions also suggest that the vehicle should proceed with caution once the light changes.
 $A_{control}$: stop
 A_{turn} : none
 A_{lane} : none

Figure 13. A successful annotation example where the rainy condition and red traffic light are correctly identified, resulting in high-quality annotations.



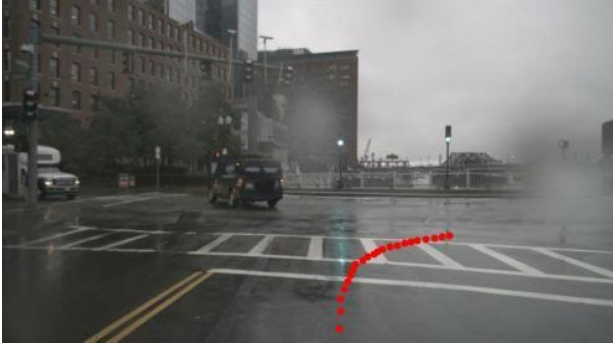
A_c : The ego vehicle is likely moving forward at a moderate speed.
 A_f : The ego vehicle will continue to move forward along the road.
 A_r : The road ahead is clear, and there are no visible obstacles or traffic signals that would necessitate stopping. The white van is not in the direct path of the ego vehicle, allowing it to proceed safely.
 $A_{control}$: go straight
 A_{turn} : none
 A_{lane} : none

Figure 12. A successful annotation example where the white van is correctly identified as irrelevant to the ego vehicle's driving.



A_c : The ego vehicle is currently stopped or moving very slowly at an intersection.
 A_f : The ego vehicle is likely to proceed forward and make a slight right turn.
 A_r : The traffic light is green, indicating it is safe to proceed. The road ahead is clear, with no visible obstacles or traffic, allowing the vehicle to move forward and follow the road's curve to the right.
 $A_{control}$: go straight
 A_{turn} : turn left
 A_{lane} : none

Figure 14. An imperfect annotation example where reasoning annotations are accurate but the turn action is incorrectly annotated as "turn left".



A_c : The ego vehicle is currently stopped or moving very slowly at the intersection.

A_f : The ego vehicle is likely to proceed through the intersection, making a right turn.

A_r : The vehicle is positioned at a stop line, indicating it is waiting for a safe opportunity to proceed. The intersection appears clear, and the vehicle is aligned to make a right turn, which is a common maneuver at intersections when clear.

$A_{control}$: move slowly

A_{turn} : turn right

A_{lane} : none

Figure 15. An imperfect annotation example where an overly cautious annotation is generated, despite the ego vehicle continuing without stopping or slowing down.



A_c : The ego vehicle is likely stopped or moving very slowly at the intersection.

A_f : The ego vehicle will remain stopped or proceed very slowly until the traffic light changes to green.

A_r : The red traffic light indicates that the ego vehicle must stop to allow cross traffic to pass safely. The presence of the van crossing the intersection further supports the need for the ego vehicle to wait until it is safe to proceed.

$A_{control}$: stop

A_{turn} : none

A_{lane} : none

Figure 16. An imperfect annotation example where the pedestrian traffic light is mistakenly considered, leading to an incorrect stop annotation.

In Fig. 15, the VLM outputs “stop” or “move slowly” as the ego vehicle’s current status. While these outputs are plausible, they are inconsistent with the ground truth, as the projected future trajectory indicates that the ego vehicle is currently turning right at the intersection. On the other hand, the action annotation successfully predicts the correct future action.

In Fig. 16, the VLM mistakenly identifies the red pedestrian light as a traffic light and provides incorrect responses.

Overall, despite making occasional mistakes, the VLM demonstrates the ability to generate meaningful annotations that uncover the underlying rationale behind driving decisions, bringing benefits to our proposed method as validated by our experiments. By querying two independent annotation questions, our method is robust to VLM mistakes that often appear in only one of the two responses, as seen in Fig. 14 and Fig. 15. We defer to obtaining more accurate VLM responses as future work to further advance the performance of E2E planning models.

C. Additional Qualitative Examples

We present an enhanced version of Fig. 4 through a set of individual figures: Fig. 17, Fig. 18, Fig. 19, and Fig. 20, where each figure includes the full 6 camera images from the dataset, although our VLM annotation pipeline only focuses on the front-view image, as discussed in Sec. 3.1.

In addition to Fig. 4, we provide four extra qualitative examples to compare the planning results of our proposed method against UniAD, as shown in Fig. 21, Fig. 22, Fig. 23, and Fig. 24.

In Fig. 21 and Fig. 22, the planning trajectories generated by UniAD are winding, lack smoothness, and fail to stay within the center of the lane. In contrast, our method produces trajectories that are significantly smoother and stay within the lane boundaries.

Similarly, in Fig. 23 and Fig. 24, the commands generated by UniAD are incorrect, as the ego vehicle is moving forward. However, our action head successfully predicts the correct actions in these scenarios.

These qualitative examples highlight the capability of VLM-AD to produce smoother and more accurate planning trajectories in challenging driving scenarios, while also providing enhanced interpretability.



(a) UniAD.



(b) VLM-AD (Ours).

Figure 17. Our method generates a smooth trajectory for an evening driving scenario, in contrast to the baseline method that predicts a winding trajectory.

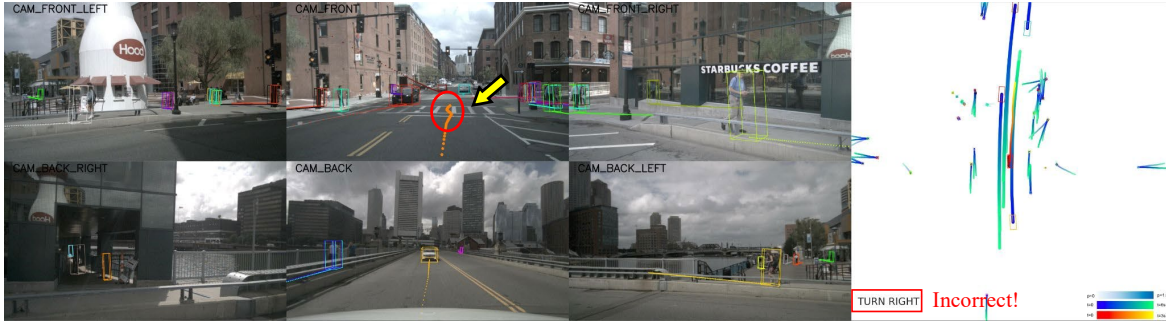


(a) UniAD.

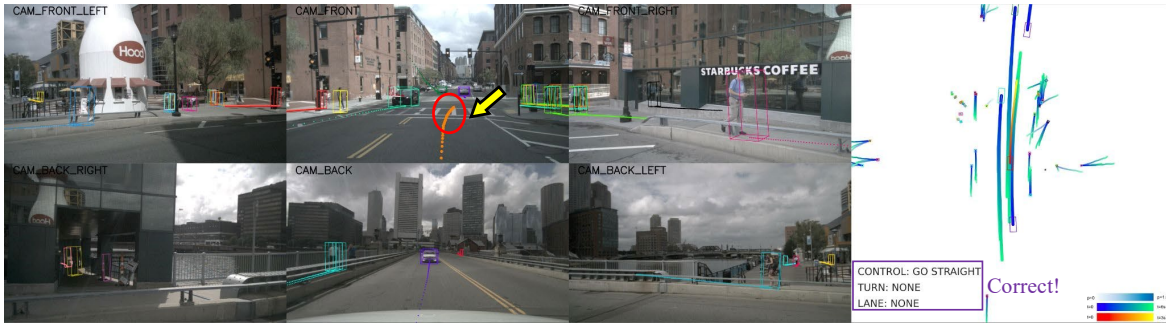


(b) VLM-AD (Ours).

Figure 18. Our method accurately predicts the correct actions when driving on a curved road, while the command generated by UniAD is incorrect.



(a) UniAD.



(b) VLM-AD (Ours).

Figure 19. Our method predicts accurate actions and a smooth trajectory in an urban driving scenario, in contrast to the baseline method that predicts a winding trajectory based on an incorrect command.

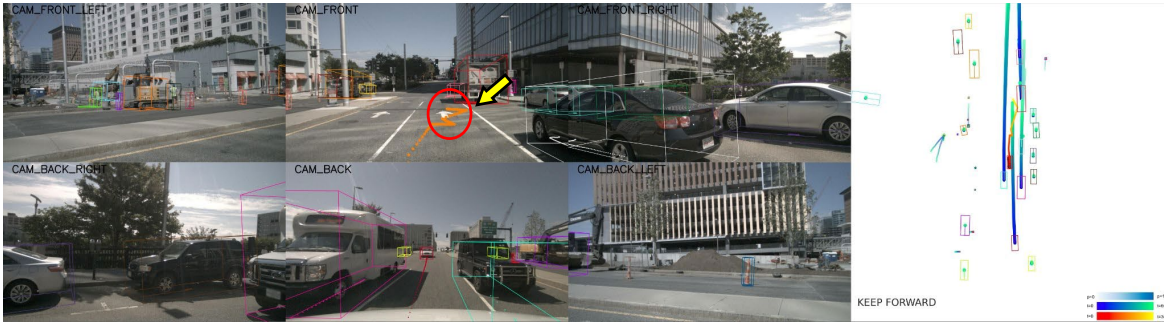


(a) UniAD.

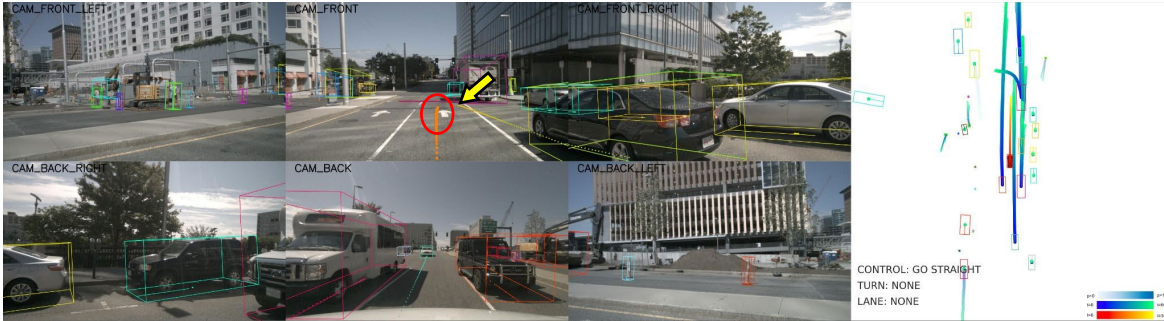


(b) VLM-AD (Ours).

Figure 20. Our method predicts accurate actions and a smooth trajectory in rainy conditions, in contrast to the baseline method that predicts a winding trajectory based on an incorrect command.



(a) UniAD.

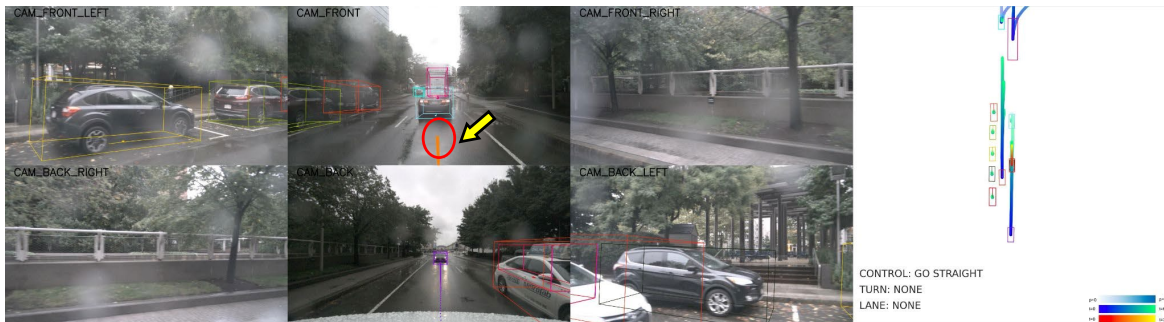


(b) VLM-AD (Ours).

Figure 21. Our method predicts an accurate trajectory that stays within the lane boundaries, in contrast to the baseline method that predicts a zigzagging trajectory.



(a) UniAD.



(b) VLM-AD (Ours).

Figure 22. Our method predicts a smooth trajectory that stays within the lane boundaries, in contrast to the baseline method that predicts a swerving trajectory.



(a) UniAD.



(b) VLM-AD (Ours).

Figure 23. The baseline model predicts an accurate trajectory but is based on an incorrect command, while our method predicts both accurate actions and a precise future trajectory.



(a) UniAD.



(b) VLM-AD (Ours).

Figure 24. The baseline model predicts an accurate trajectory but is based on an incorrect command, while our method predicts both accurate actions and a precise future trajectory.